Supplementary material for: Exceptional contours and band structure design in parity-time symmetric photonic crystals

Alexander Cerjan, Aaswath Raman, and Shanhui Fan*
Department of Electrical Engineering, and Ginzton Laboratory, Stanford University, Stanford, California 94305, USA
(Dated: March 26, 2016)

I. VECTORIAL FORM OF THE $\mathbf{k}\cdot\mathbf{p}$ PERTURBATION THEORY

In the main text of the Letter, we present a derivation of a $\mathbf{k}\cdot\mathbf{p}$ perturbation theory for the TM bands of two-dimensional photonic crystals (PhCs). Here, we provide the same derivation for the vectorial form of the $\mathbf{k}\cdot\mathbf{p}$ theory. While most of the steps are identical, the basis of states used in the expansion

$$\mathbf{E}_{n\mathbf{k}}(\mathbf{x}) = \sum_m C_{nm}(\mathbf{k}) e^{i(\mathbf{k}-\mathbf{k}_0)\cdot\mathbf{x}} \mathbf{E}^{(0)}_{m\mathbf{k}_0}(\mathbf{x}), \tag{S1}$$

must now also include non-physical states with $\omega^{(0)}_m = 0$ to satisfy the divergence condition [1]. However, this subtle difference does not alter the form of the resulting matrix equation,

$$\sum_m \left[\left(\omega^2_n(\mathbf{k}) - (\omega^{(0)}_m(\mathbf{k}_0))^2 \right) \frac{\delta_{lm}}{c^2} + i\tau \frac{\omega^2_n(\mathbf{k})}{c^2} G_{lm} - sP_{lm} + s^2 Q_{lm} \right] C_{nm}(\mathbf{k}) = 0, \tag{S2}$$

where $\mathbf{s} = \mathbf{k} - \mathbf{k}_0 \equiv s\hat{\mathbf{s}}$. The gain and loss coupling elements are given by

$$G_{lm} = \int_{\mathrm{SC}} g(\mathbf{x}) \left(\mathbf{E}^{(0)}_{l\mathbf{k}_0}(\mathbf{x}) \right)^* \cdot \mathbf{E}^{(0)}_{m\mathbf{k}_0}(\mathbf{x}) d\mathbf{x}, \tag{S3}$$

while the elements P_{lm} and Q_{lm} are now

$$P_{lm} = i \int_{\mathrm{SC}} \left(\mathbf{E}^{(0)}_{l\mathbf{k}_0}(\mathbf{x}) \right)^* \cdot \left[\hat{\mathbf{s}} \times \nabla \times + \nabla \times \hat{\mathbf{s}} \times \right] \mathbf{E}^{(0)}_{m\mathbf{k}_0}(\mathbf{x}) d\mathbf{x}, \tag{S4}$$

$$Q_{lm} = \int_{\mathrm{SC}} \left(\mathbf{E}^{(0)}_{l\mathbf{k}_0}(\mathbf{x}) \right)^* \cdot \left(\hat{\mathbf{s}} \times \hat{\mathbf{s}} \times \mathbf{E}^{(0)}_{m\mathbf{k}_0}(\mathbf{x}) \right) d\mathbf{x}. \tag{S5}$$

The vectorial form of the coupling elements, Eqs. (S3)-(S5), still obey the same selection rules as their TM counterparts.

II. RESTRICTIONS ON THE MATRIX COUPLING ELEMENTS

In this section, we provide the proof of the statement made in the main text of the Letter, that P_{lm} and Q_{lm} as defined in Eqs. (S4) and (S5) only couple wave functions of the Hermitian system which satisfy the hidden translational symmetry relationship, Eq. (5) from the main text, for the same $\mathbf{L}_j$. Just as there are N elements of the set $\{\mathbf{L}\}$ which generate the primitive Brillouin zone from the supercell Brillouin zone, there are N translation vectors $\{\mathbf{c}\}$ which generate the supercell from the primitive cell. Only one of these elements of $\{\mathbf{c}\}$ lies in both the primitive cell and the supercell, which we choose to index as the first element in the set, typically $\mathbf{c}_1 = \mathbf{0}$. Together, these obey the discrete Fourier relation [2]

$$\frac{1}{N} \sum_{n=1}^{N} e^{i(\mathbf{L}_i - \mathbf{L}_j)\cdot\mathbf{c}_n} = \delta_{ij}. \tag{S6}$$

* shanhui@stanford.edu

To begin, the integral defining P_{lm}, Eq. (S4), can be broken up into integrals over the constituent primitive cells that together comprise the supercell,

$$P_{lm} = i\sum_{n=1}^{N}\int_{\mathrm{PC}_n}\left(\mathbf{E}^{(0)}_{l\mathbf{k}_0}(\mathbf{x})\right)^*\cdot[\hat{\mathbf{s}}\times\nabla\times+\nabla\times\hat{\mathbf{s}}\times]\,\mathbf{E}^{(0)}_{m\mathbf{k}_0}(\mathbf{x})d\mathbf{x}, \tag{S7}$$

where PC_n is the primitive cell associated with the translation vector $\mathbf{c}_n$. Next, noting that every supercell band originating from the same unfolded band in the primitive Brillouin zone will satisfy Eq. (5) for a different $\mathbf{L}$, we choose to relabel the wavefunction indices as $m = (\nu, j)$, $l = (\nu', j')$, where ν is the corresponding index of the unfolded band in the primitive Brillouin zone and the supercell wavefunction obeys Eq. (5) for $\mathbf{L}_j$. Thus,

$$\begin{aligned}
&\int_{\mathrm{PC}_n}\left(\mathbf{E}^{(0)}_{\nu',j',\mathbf{k}_0}(\mathbf{x})\right)^*\cdot[\hat{\mathbf{s}}\times\nabla\times+\nabla\times\hat{\mathbf{s}}\times]\mathbf{E}^{(0)}_{\nu,j,\mathbf{k}_0}(\mathbf{x})d\mathbf{x}\\
&\qquad=\int_{\mathrm{PC}_1}\left(\mathbf{E}^{(0)}_{\nu',j',\mathbf{k}_0}(\mathbf{x}+\mathbf{c}_n)\right)^*\cdot[\hat{\mathbf{s}}\times\nabla\times+\nabla\times\hat{\mathbf{s}}\times]\,\mathbf{E}^{(0)}_{\nu,j,\mathbf{k}_0}(\mathbf{x}+\mathbf{c}_n)d\mathbf{x}\\
&\qquad=e^{i(\mathbf{L}_j-\mathbf{L}_{j'})\cdot\mathbf{c}_n}\int_{\mathrm{PC}_1}\left(\mathbf{E}^{(0)}_{\nu',j',\mathbf{k}_0}(\mathbf{x})\right)^*\cdot[\hat{\mathbf{s}}\times\nabla\times+\nabla\times\hat{\mathbf{s}}\times]\,\mathbf{E}^{(0)}_{\nu,j,\mathbf{k}_0}(\mathbf{x})d\mathbf{x},
\end{aligned} \tag{S8}$$

in which we have used the fact that the derivative operator is invariant under translations. Inserting this result back in to Eq. (S7), we can use the discreet Fourier property to find

$$\begin{aligned}
&i\sum_{n=1}^{N}\int_{\mathrm{PC}_n}\left(\mathbf{E}^{(0)}_{l\mathbf{k}_0}(\mathbf{x})\right)^*\cdot[\hat{\mathbf{s}}\times\nabla\times+\nabla\times\hat{\mathbf{s}}\times]\mathbf{E}^{(0)}_{m\mathbf{k}_0}(\mathbf{x})d\mathbf{x}\\
&\qquad=i\sum_{n=1}^{N}e^{i(\mathbf{L}_j-\mathbf{L}_{j'})\cdot\mathbf{c}_n}\int_{\mathrm{PC}_1}\left(\mathbf{E}^{(0)}_{\nu',j',\mathbf{k}_0}(\mathbf{x})\right)^*\cdot[\hat{\mathbf{s}}\times\nabla\times+\nabla\times\hat{\mathbf{s}}\times]\,\mathbf{E}^{(0)}_{\nu,j,\mathbf{k}_0}(\mathbf{x})d\mathbf{x}\\
&\qquad=iN\delta_{jj'}\int_{\mathrm{PC}_1}\left(\mathbf{E}^{(0)}_{\nu',j',\mathbf{k}_0}(\mathbf{x})\right)^*\cdot[\hat{\mathbf{s}}\times\nabla\times+\nabla\times\hat{\mathbf{s}}\times]\,\mathbf{E}^{(0)}_{\nu,j,\mathbf{k}_0}(\mathbf{x})d\mathbf{x},
\end{aligned} \tag{S9}$$

which yields the desired result,

$$P_{(\nu',j'),(\nu,j)} \propto \delta_{jj'}. \tag{S10}$$

A very similar proof can be given for the elements Q_{lm}, resulting in

$$Q_{(\nu',j'),(\nu,j)} \propto \delta_{jj'}. \tag{S11}$$

III. BAND MERGING RATIOS

In the main text, the thresholdless $\mathcal{PT}$ transition is observed in the increase of the range of incident angles which yield non-unitary behavior for a single frequency, as shown in Fig. 2(a). However, the $\mathcal{PT}$ transition can also be seen in supercell PhCs by monitoring the ratio of the proportion of wavevector space for a pair of bands which have merged to the total area as a function of the applied gain and loss to the system. This process is shown in Fig. S1 for the same system which is studied in Fig. 1 of the main paper. Here, the first pair of bands (blue) is the same set of bands shown in Figs. 1(c), and (e), while the third pair of bands (yellow) correspond to those from Figs. 1(d), and (f). As expected, increasing the gain and loss in the system increases the proportion of merged wavevector space. Furthermore, higher order bands are seen to merge more quickly than lower order bands.

IV. UNIDIRECTIONAL BEHAVIOR

Similar to many other $\mathcal{PT}$ systems, supercell $\mathcal{PT}$ symmetric PhCs can also exhibit unidirectional behavior. To demonstrate this, we study a PhC slab based upon the 2D crystal shown in Fig. 1(a) that is infinite in the y-direction, while containing 24 layers in the x-direction, and compare the behavior of the structure when the first layer illuminated is a gain layer versus a loss layer, as shown in Figs. S2(a) and S2(b). For the former structure, the normalized transmission, reflection, and non-unitary behavior are shown in Figs. S2(c)-S2(e), and this can be easily visually

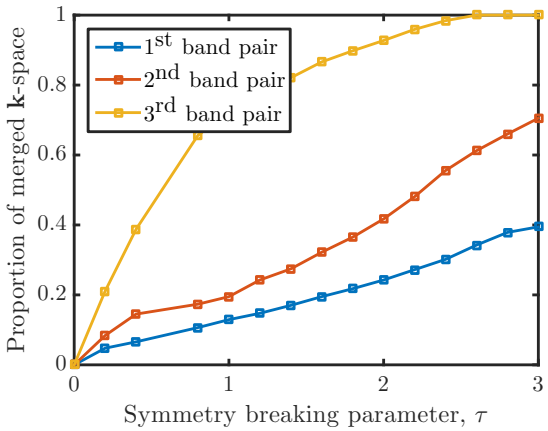

FIG. S1. Plot of the ratio of merged wavevector space to total area as a function of the gain/loss parameter τ for the PhC comprised of square rods with side length $0.6a$ of dielectric, $\varepsilon_{die} = 12$, embedded in air, $\varepsilon_{air} = 1$, with a square primitive cell side length of a. This is the same crystal as is shown in Fig. 1. The ratio for the three lowest frequency pairs of bands are shown in blue, red, and yellow respectively.

contrasted with the same quantities for the latter structure in Figs. S2(f)-S2(h). While the normalized transmission is seen to be similar between the two structures, with minor differences at larger frequencies, the normalized reflection and net non-unitary behavior is seen to be quite different, demonstrating dependence upon the choice of structure orientation.

V. ANTI-SYMMETRIC DISTRIBUTION OF LOSS

Similar to most experimental observations of $\mathcal{PT}$ physics in other systems, it is likely that the simplest experimental design to observe the phenomena predicted here is using a system where the supercell is creating using an anti-symmetric distribution of no-loss and double-loss as shown in Fig. S3(a), rather than the analogous distribution of gain and loss shown in Fig. 1(a). In the literature, the difference between these two setups is typically treated as adding a constant amount of loss to the entire system, which does not effect the location of the exceptional point in coupled mode theories of $\mathcal{PT}$ systems. However, this is not true when solving for the band structure of a PhC using the wave equation for two reasons. First, in the case of the PhCs studied in the main text, only portions of the crystal contain gain or loss, as the remainder of the crystal is comprised of air. Thus,

$$\varepsilon_{loss}(\mathbf{x}) \neq \varepsilon_{\mathcal{PT}}(\mathbf{x}) + i\tau, \tag{S12}$$

as the air regions should not be made to be lossy. Here, $\varepsilon_{\mathcal{PT}}$ is the dielectric of the total non-Hermitian system.

It would seem that this problem could be easily fixed by instead defining the dielectric of such an anti-symmetric lossy PhC as

$$\varepsilon_{loss}(\mathbf{x}) = \varepsilon(\mathbf{x}) + i\tau h(\mathbf{x}), \tag{S13}$$

where $\varepsilon(\mathbf{x})$ is the dielectric of the underlying passive system and $h(\mathbf{x})$ is either 0, for both the no-loss elements in the dielectric material and the air, or 2 in the lossy dielectric elements. However, this does not work either for a more subtle reason. In this circumstance, the confinement provided by the dielectric elements is no longer equal, the lossy elements offer increased index contrast relative to the surrounding air. Thus, the lossy system does not perfectly replicate the features of the corresponding $\mathcal{PT}$ system, and such a lossy system will not pass through an exceptional point strictly through increasing τ. In general, the exceptional point can be restored by tuning an additional parameter of the system, such as the relative size of the passive and lossy dielectric elements.

Despite this difficulty, no-loss / double-loss systems described by Eq. (S13) still exhibit nearly all of the interesting features of the corresponding $\mathcal{PT}$ system without any additional tuning, such as flat isofrequency contours suitable for supercollimation and sharp boundaries for observing a non-unitary superprism effect. These features can be seen in Figs. S3(b) and (c), which show the same pairs of bands for the lossy system as are shown for the corresponding $\mathcal{PT}$ system in Figs. 1(e) and (f). In fact, the only qualitative difference between these two systems is that a small gap opens between the flat regions in the upper and lower bands, such that the nearly loss-less state localized on

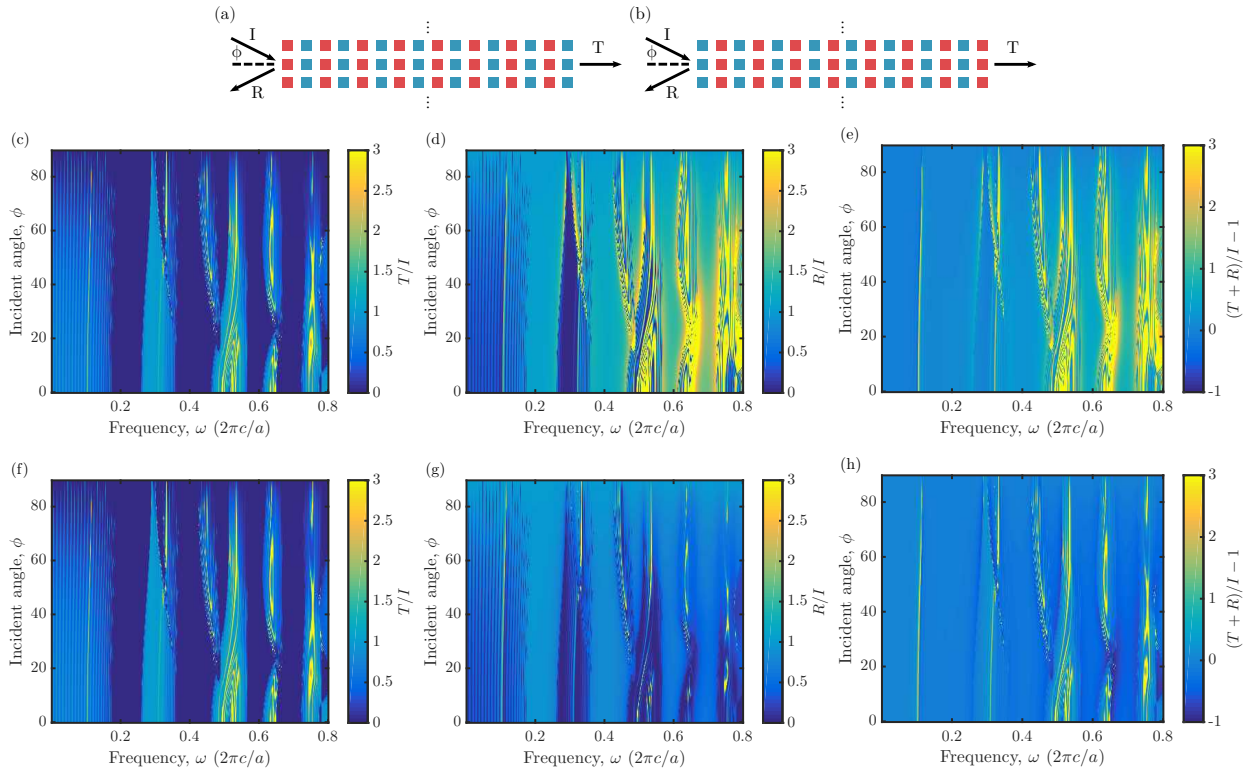

FIG. S2. (a-b) Schematics of the 2D PhC comprised of square rods with side length $0.6a$, $\varepsilon_{die} = 12$ and $\tau = 0.6$, embedded in air, $\varepsilon_{air} = 1$, with a square primitive cell side length of a, which is infinite in the transverse direction, and contains 24 layers in the longitudinal direction. The only difference between the two structures is in whether the first layer is chosen to be gain (a) or loss (b). (c-e) Normalized transmission, reflection, and non-unitary behavior as a function of frequency and incident angle of the PhC slab from (a) when illuminated with a plane wave source. (f-h) Normalized transmission, reflection, and non-unitary behavior as a function of frequency and incident angle of the PhC slab from (b) when illuminated with a plane wave source. Values of 0 indicate unitary behavior, while any other value represents non-unitary behavior. The reflection and transmission coefficients were calculated using the Fourier Modal Method as implemented in S^4 [3].

the passive dielectric elements has a slightly different frequency than the very lossy state localized on the absorbing dielectric elements. This gap can be seen in Fig. S3(d) for the same pair of bands as are shown in Fig. S3(b). Thus, it should be possible to observe all of the essential phenomena predicted here in the corresponding lossy system, which could be fabricated using existing semiconductor technologies, with the loss either added by including a quantum well layer or quantum dots, or through using another material with latent absorptive properties.

[1] J. E. Sipe, Phys. Rev. E **62**, 5672 (2000).
[2] P. B. Allen, T. Berlijn, D. A. Casavant, and J. M. Soler, Phys. Rev. B **87**, 085322 (2013).
[3] V. Liu and S. Fan, Computer Physics Communications **183**, 2233 (2012).

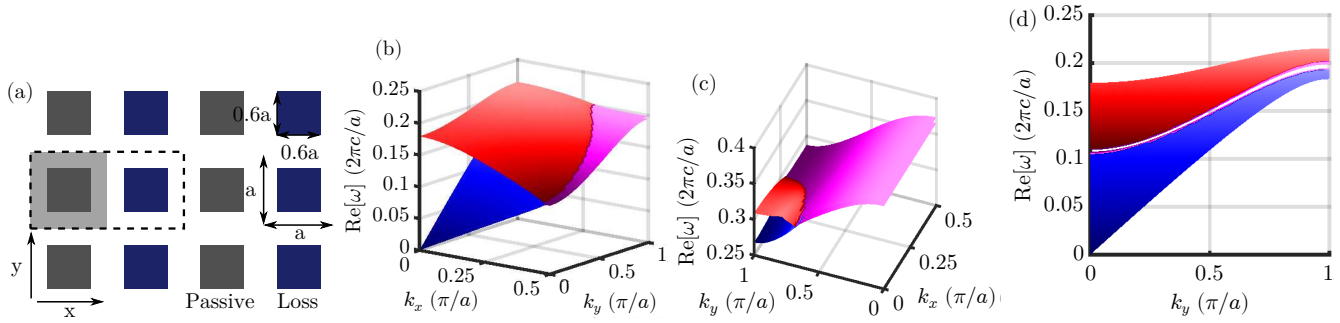

FIG. S3. (a) Schematic of the 2D PhC comprised of square rods with side length $0.6a$ of dielectric, $\varepsilon_{die} = 12$, embedded in air, $\varepsilon_{air} = 1$, with a square primitive cell side length of a. The primitive cell is indicated in gray, while the supercell contains two primitive cells and is marked with a dashed border. When $\tau \neq 0$, the dark grey rods remain passive, while the deep blue rods contain loss. (b) Real part of the frequencies for the first (blue) and second (red) supercell TM bands when $\tau = 1.5$. (c) Real part of the frequencies for the fifth (blue) and sixth (red) supercell TM bands when $\tau = 1.5$. (d) Same bands as (b), but shown from a different orientation.